Cellulose nanocrystal-based films produced by more sustainable extraction protocols from *Posidonia oceanica* waste biomass

*Isaac Benito-González, Amparo López-Rubio, Rafael Gavara, Marta Martínez-Sanz**

Food Safety and Preservation Department, IATA-CSIC, Avda. Agustín Escardino 7, 46980 Paterna, Valencia, Spain

**Corresponding author: Tel.: +34 963200022; fax: +34 963636301*

E-mail address: mmartinez@iata.csic.es

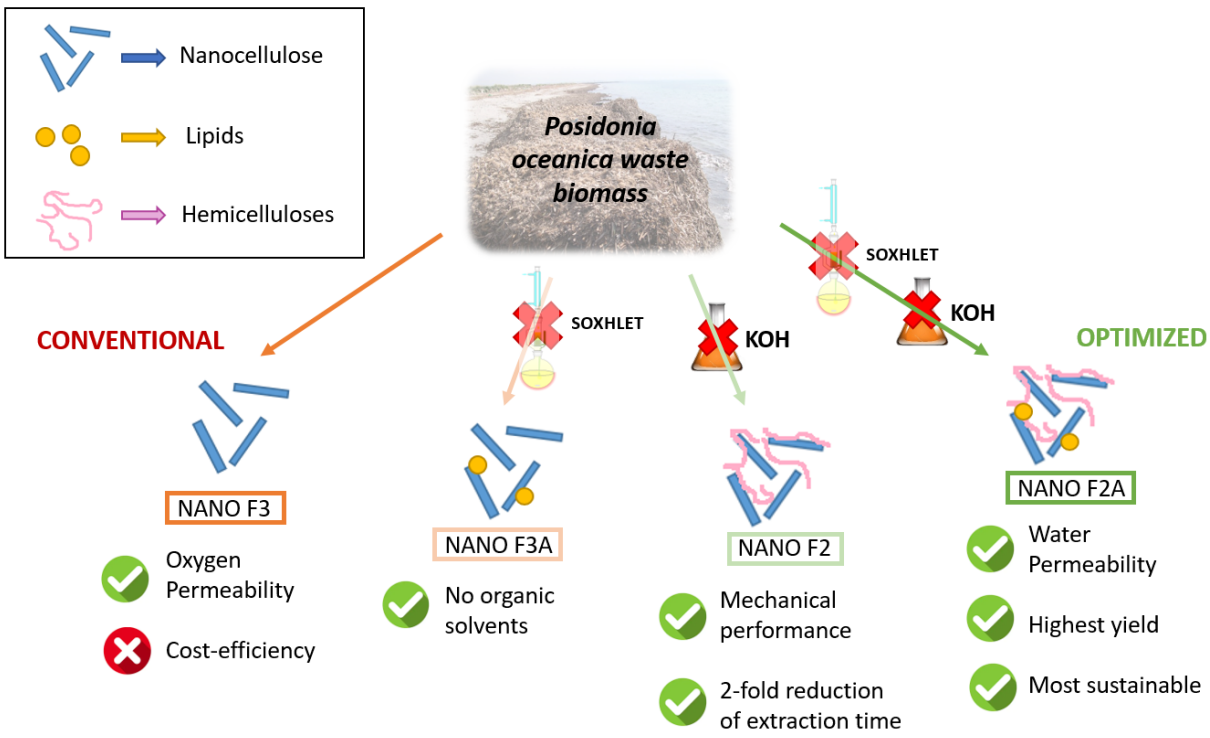

Abstract

Simplified extraction procedures (avoiding Soxhlet treatment and/or hemicellulose removal) were evaluated to valorize waste biomass from *Posidonia oceanica* leaves, obtaining cellulosic fractions and nanocrystals, which were subsequently used to produce films from their aqueous suspensions. Cellulose purification significantly improved mechanical and barrier properties of the films obtained from the fractions, while the extracted nanocrystals yielded films with remarkably improved properties, outperforming most benchmark biopolymers. The lipids initially present in the fractions without Soxhlet treatment were not completely digested by the hydrolysis treatment, having a positive impact on the water vapor permeability of the films (up to 63% drop), although negatively impacting oxygen permeability (increased by 20-30-fold). On the contrary, some hemicelluloses present in the less purified fractions, strongly interacting with cellulose, remained in the extracted nanocrystals leading to enhanced mechanical properties (45% higher tensile strength and 2-fold increase in the elongation at break), but lower water barrier (up to 70% higher permeability than the pure cellulose nanocrystals) due to their hydrophilic character. Films produced from the less purified nanocrystals showed the best compromise between mechanical and barrier performance, while offering a great advantage in terms of sustainability and reduced costs.

Keywords: seagrass; nanocellulose; hemicelluloses; biopolymers; XRD.

1. Introduction

Petroleum-based plastics have been extensively used during the last decades within the food packaging area because of their low-cost, good processability and tailored barrier and mechanical performance. However, besides the sustainability issues derived from the use of fossil fuels, the large amounts of waste generated as a result of their disposal derive in a severe environmental impact, since conventional plastics can take thousands of years to degrade, endangering terrestrial and aquatic ecosystems. Although recycling strategies contribute to palliate this problem, they are far from providing a long-term sustainable solution. As an alternative to petroleum-based plastics, biodegradable polymers derived from renewable resources, i.e. biopolymers, have been developed during the lasts years. Nevertheless, most biopolymers present significant drawbacks when compared to benchmark synthetic polymers, such as lower barrier and mechanical performance, as well as higher production costs. Furthermore, most of the starting raw materials are vegetable sources, whose utilization for the production of biopolymers competes with their primary use as food sources. In this context, the valorization of aquatic biomass, such as algae and aquatic plants, available in large quantities, represents an efficient alternative to the use of land biomass. These sources have been reported to contain large amounts of carbohydrates, which could be interesting for the development of bio-based plastics (Benito-González et al. 2018; Martínez-Sanz et al. 2018; Ray and Lahaye 1995; Siddhanta et al. 2009).

In particular, *Posidonia oceanica*, one of the most abundant aquatic plant species in the Mediterranean Sea, has been demonstrated to be an optimum source for the extraction of cellulose and lignocellulosic fractions with promising properties for the development of cellulose-based packaging materials or to be used as fillers to enhance the properties of other

biopolymers (Benito-González et al. 2018; Benito-González et al. 2019; Bettaieb et al. 2015; Fortunati et al. 2015). During its lifecycle, *Posidonia* leaves detach off the stems and are transported towards the sea shores by marine currents, giving rise to a residue that affects the quality of the beaches (Balata and Tola 2017) and generating costs to local authorities associated to its collection and disposal to landfills. Therefore, the utilization of this residue for the extraction of lignocellulosic materials would be particularly interesting and in line with circular economy policies.

Although cellulose itself has interesting properties for food packaging applications, its treatment by acid hydrolysis digests the amorphous domains, yielding highly crystalline nanocellulose or cellulose nanocrystals (Bettaieb et al. 2015; Chen et al. 2016). These nanocrystals feature an attractive combination of properties such as biocompatibility, large specific surface area and aspect ratio, high elastic modulus, high thermal stability and excellent optical transparency (Dufresne 2006), which have been exploited to improve the properties of other biopolymer matrices, such as poly(lactic acid) (PLA) (Fortunati et al. 2015; Lizundia et al. 2016), polyhydroxyalkanoates (PHAs) (Arrieta et al. 2014; Seoane et al. 2016), polyisoprene (Siqueira et al. 2010) and pea starch (Cao et al. 2008). Besides their utilization as nanofillers, cellulose nanocrystals themselves can be used to produce high-barrier films (Martínez-Sanz et al. 2013), although this approach has not been fully explored to date.

Despite most of the works available on the literature focus on achieving a complete purification of cellulose from its raw source, it has been recently reported that less purified lignocellulosic fractions may also possess interesting properties for their use in packaging materials (Benito-González et al. 2018; Martínez-Sanz et al. 2018). Using less purification steps to generate these fractions allows reducing the energy and time consumption, minimizing the economic gap between biopolymers and conventional fossil-fuel derived plastics.

In this work, the waste biomass from *Posidonia oceanica* leaves has been valorized as a natural source of cellulosic fractions and nanocrystals extracted by acid hydrolysis, while exploring the possibility of suppressing processing steps on the purification process. Aqueous suspensions from the different fractions and nanocrystals have been used to generate films and their structural and functional properties have been characterized to select the most promising materials for food packaging applications, while minimizing the processing steps to achieve more sustainable and economically viable materials. Our hypothesis is that reducing the purification steps may not only diminish the production costs and environmental impact, but also yield novel high-performance cellulose-based biopolymeric films able to replace petroleum-based polymers in food packaging.

2. Materials and methods

2.1. Raw materials

Posidonia oceanica leaf biomass was gathered from coastal areas in the Mediterranean sea, as reported in (Benito-González et al. 2018). The composition of the raw biomass, obtained from previous analyses, is shown in Figure 1.

2.2. Preparation of cellulosic fractions

A purification procedure described in previous work (Benito-González et al. 2018; Martínez-Sanz et al. 2015b) was carried out to sequentially remove cell wall components and obtain pure cellulose. The general protocol, as well as the specific process parameters, are schematically shown in Figure 1. Briefly, this process consisted of an initial Soxhlet extraction to remove pigments and lipids, followed by a treatment with $NaClO_2$ to remove lignin (yielding F2 fraction) and a final alkaline treatment with KOH to remove the hemicelluloses (yielding F3

fraction). The possibility of suppressing the initial Soxhlet treatment was also evaluated, obtaining two additional fractions, one after treating the biomass with $NaClO_2$ (referred to as F2A) and another fraction after the treatment with KOH (designated as F3A). All the fractions (F2, F2A, F3 and F3A) were obtained as a partially hydrated gel-like material that was stored in the refrigerator until further use.

2.3. Preparation of cellulosic nanocrystals

The cellulosic fractions were used as starting materials for the production of nanocrystals by means of acid hydrolysis (cf. Figure 1). An optimized method, previously applied for the extraction of cellulose nanocrystals from bacterial cellulose (Martínez-Sanz et al. 2011), with some minor modifications, was applied. Briefly, the gel-like lignocellulosic fractions were immersed in a H_2SO_4 solution (30%w/w), with a ratio of 1.5 g dry fraction/100 mL H_2SO_4, at 50ºC and stirred for 2 hours. After that, the material was subjected to several centrifugation and washing cycles to remove the acid and the pH was adjusted to 7 with NaOH. The obtained nanocrystals (labelled as NANO F2, NANO F2A, NANO F3 and NANO F3A, depending on the fraction used as the starting material) were stored in the fridge as partially hydrated gel-like materials, until further use.

2.4. Production of cellulosic films

Cellulosic films were produced by dispersing 0.25-0.5 g of cellulosic fractions or cellulosic nanocrystals in 50 mL of distilled water. The aqueous suspensions were vacuum filtered using PTFE filters (0.2 μm pore) and the solid fraction remaining in the filter was dried at room temperature overnight (20ºC, 40% RH). The obtained films were stored in equilibrated relative humidity cabinets at 0% RH and 25ºC for three days prior to their characterization.

131 2.5. Attenuated total reflectance (ATR) FT-IR analysis

132 Freeze-dried fractions and nanocrystals were analysed by FT-IR in attenuated total reflectance
133 (ATR) mode using a Thermo Nicolet Nexus (GMI, USA) equipment. The spectra were taken
134 at 4 cm^{-1} resolution in a wavelength range between 400-4000 cm^{-1} and averaging a minimum
135 of 32 scans.

136

137 2.6. ^{13}C CP/MAS Nuclear Magnetic Resonance (NMR) spectroscopy

138 The solid-state 13C CP/MAS NMR experiments were performed at a ^{13}C frequency of 100.63
139 MHz on a WB-AVIII Bruker spectrometer. The samples were packed in a 4-mm, PSZ
140 (partially-stabilized zirconium oxide) rotor with a perfluorinated polymer (KelF) end cap. The
141 rotor was spun at 10 kHz at the magic angle (54.7º). The 90º pulse width was 2.2 μs and a
142 contact time of 2 ms was used for all samples with a recycle delay of 5 s. The spectral width
143 was 30 kHz, acquisition time 34 ms, time domain points 2k, transform size 8k and line
144 broadening 10 Hz. 20k scans were accumulated for each spectrum. Spectra were referenced to
145 external glycine.

146

147 2.7. Scanning electron microscopy (SEM)

148 SEM characterization was carried out on a Hitachi microscope (Hitachi S-4800) at an
149 accelerating voltage of 10 kV and a working distance of 8-16 mm. Small samples (~5 mm^2
150 area) of the cellulosic films were cut to observe their surface. The samples were then sputtered
151 with a gold–palladium mixture under vacuum during 3 minutes.

152

153 2.8. Transmission electron microscopy (TEM)

One drop (8 μL) of a 0.001% aqueous suspension of the different nanocrystals was allowed to dry on a carbon coated grid (200 mesh). The nanocrystals were then stained with uranyl acetate. TEM was performed using a JEOL 1010 at an accelerating voltage of 80 kV.

2.9. Water vapour permeability (WVP) and water uptake

Water vapour permeability and water uptake values were estimated by registering the weight gain of film samples as a function of time when being exposed to 75% RH and 25 °C conditions. The detailed protocols are described in (Benito-González et al. 2018).

2.10. Oxygen permeability

O_2 permeability values in dry conditions were obtained by an isostatic method based on a permeation cell connected in series to a gas chromatograph (GC) equipped with a thermal conductivity detector (TCD) as described elsewhere (Cerisuelo et al. 2012). In brief, the film under analysis separates the two chambers of the permeation cell (Film area was 5 cm^2). In the low concentration chamber, a constant flow of nitrogen carries the permeated molecules out of the cell and to the injection valve of the GC. In the high concentration chamber, a constant flow of oxygen maintains the pressure of the gas constant at 1 atm. Gas pressures were adjusted by appropriate manometers and flows were controlled by needle valves and measured by mass flowmeters from Dakota Instruments (New York). Gas samples of the nitrogen flow stream were injected until peak area got constant, indicating the achievement of stationary state.

2.11. Contact angle measurements

Contact angle values were estimated from measurements performed in a Video-Based Contact Angle Meter model OCA 20 (DataPhysics Instruments GmbH, Filderstadt, Germany) at ambient conditions, as previously described in (Benito-González et al. 2018).

179

180 2.12. Optical properties

181 The transparency of the films was estimated from the internal transmittance values measured
182 using a spectrocolorimeter CM-3600d (Minolta Co., Tokyo, Japan), using the same
183 methodology described in (Martínez-Sanz et al. 2018).

184

185 2.13. Mechanical properties

186 Tensile tests were performed using a Mecmesin MultiTest 1-i (1 kN) machine (Virginia, USA)
187 equipped with the EmperorTM software. The same parameters previously described in (Benito-
188 González et al. 2018) were applied and the obtained stress-strain curves were used to calculate
189 the elastic modulus, tensile strength and elongation at break of the tested films.

190

191 2.14. X-ray diffraction (XRD)

192 XRD characterization of the films was carried out using the same experimental conditions
193 described in previous work (Benito-González et al. 2018). The crystallinity index was
194 determined by integration of the peak areas and application of the following equation:

195 $$X_C(\%) = \frac{\sum A_{Crystal}}{A_{Total}} \times 100 \quad (1)$$

196 Where A_{Total} is the sum of the areas under all the diffraction peaks and $\Sigma A_{Crystal}$ is the sum of
197 the areas corresponding to the three crystalline peaks from cellulose I. The crystallite sizes
198 were estimated from the three different lattice planes of cellulose I_β using the well-known
199 Scherrer equation:

200 $$D_{(hkl)} = \frac{k \cdot \lambda}{B_{(hkl)} \cdot \cos\theta} \quad (2)$$

2.15. Statistics

Analysis of variance (ANOVA) followed by a Tukey test were performed for the comparison of more than two data sets. Significant differences ($p \leq 0.05$) are denoted by showing the data provided in the tables with different letters.

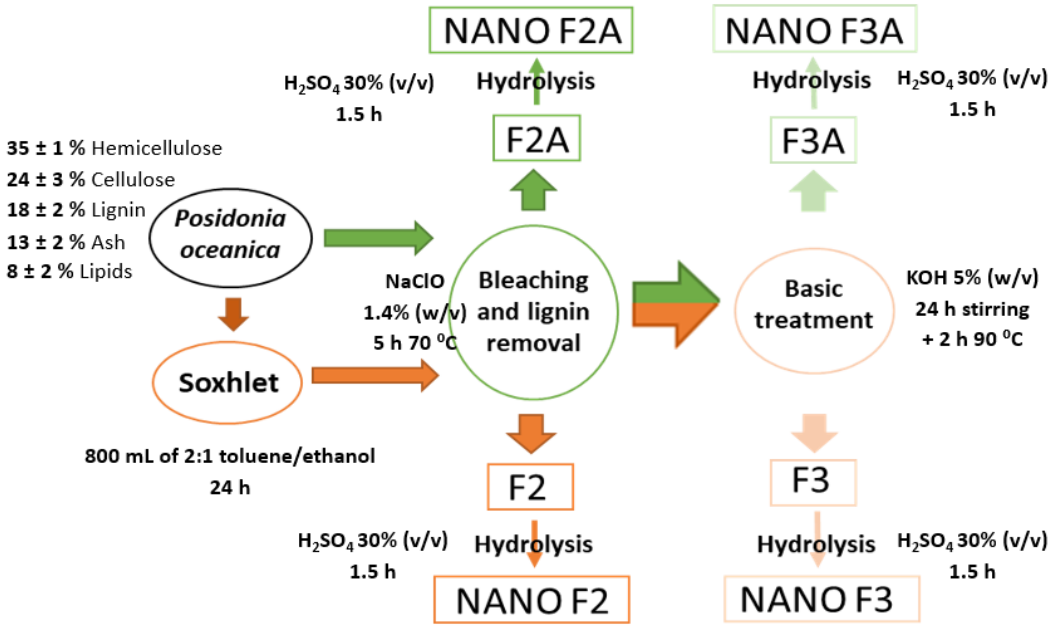

Figure 1. General protocol for the extraction of cellulosic fractions and nanocrystals from *Posidonia oceanica* waste biomass.

3. Results and discussion

3.1. Characterization of the cellulosic fractions and the extracted nanocrystals

Different cellulosic fractions were extracted from *Posidonia oceanica* biomass waste by applying a previously developed sequential extraction protocol (Benito-González et al. 2018).

According to previous results, F2 was expected to contain cellulose and hemicelluloses, while F3 was expected to consist of pure cellulose. Additionally, an alternative greener extraction protocol where the initial Soxhlet treatment was omitted (thus, avoiding the use of organic solvents), was also applied, yielding the fractions F2A and F3A. Apart from the cellulose and hemicelluloses, these two fractions were expected to contain some impurities such as lipids and pigments, which are typically removed by organic solvents during the Soxhlet treatment. The extraction yields were 50% for F2 and 25% for F3, consistent with the raw *Posidonia* composition and in agreement with previous results (Benito-González et al. 2018). As expected, the extraction yields increased slightly when omitting the Soxhlet treatment due to the presence of impurities in the material, leading to yields of 60% for F2A and 30% for F3A.

These four fractions were then subjected to an acid hydrolysis to digest the amorphous domains and isolate the crystalline fraction of the material. The yields (with respect to the raw *Posidonia* biomass) were estimated as 20%, 26%, 14% and 18% for the nanocrystals extracted from the F2, F2A, F3 and F3A fractions, respectively. Therefore, circa (ca.) 60% of the material was hydrolyzed for the F2 and F2A fractions, while only 40% of the material was hydrolyzed when using the F3 and F3A fractions. This is not surprising, since the F2 and F2A fractions contain amorphous hemicelluloses which can be easily digested by the acid. Even NANO F3 yield was consistent with others previously reported by the literature in *Posidonia oceanica* nanocrystals (Fortunati et al. 2015), and higher than others reported from different marine biomass like *Gelidium elegans* (8%) (Chen et al. 2016) or chardonnay grape-skins (Lu and Hsieh 2012).

FT-IR analyses were carried out to assess the compositional differences between the extracted fractions and the nanocrystals and the results are shown in Figure 2. As observed, several differences were evidenced in the spectra from the different fractions (cf. Figure 2A). Firstly, the intensity of several bands characteristic of hemicelluloses, such as those located at 1735, 1621 and 1533 cm^{-1} (corresponding to esters and acetyl groups) (Sun et al. 2005), which were

241 evident in the spectra from F2 and F2A, was seen to strongly decrease after the KOH treatment,
242 being hardly visible in the spectra from the F3 and F3A fractions. Moreover, some cellulose
243 characteristic peaks, such as those located at 1103, 1054 and 984 cm^{-1} (corresponding to C-C,
244 C-O, C-H stretching and C-OH bending modes (Khiari et al. 2011; Oh et al. 2005), were more
245 intense and defined in the spectra from F3 and F3A, supporting the effectiveness of the
246 cellulose purification process.

247 With regards to the Soxhlet treatment, it was seen to have a clear effect on the peaks at 2912
248 and 2845 cm^{-1}, which appeared as very sharp peaks in the spectra from F2A and, to a lesser
249 extent, F3A. These peaks correspond to the CH_2 asymmetrical and symmetrical stretching,
250 usually associated with the fatty acids aliphatic chain (Abidi et al. 2014; Freire et al. 2006).
251 This suggests that, as already anticipated, some lipidic components remained in the fractions
252 obtained without applying the Soxhlet treatment. The lower intensity of these bands in the case
253 of F3A might be due to the application of an adittional purification step (i.e., KOH treatment)
254 where some fatty acids might have been removed.

255 The spectra from the extracted nanocrystals were very similar, as shown in Figure 2B. The first
256 clear observation is that after the acid hydrolysis, all the bands arising from the presence of
257 hemicelluloses were strongly reduced, indicating that they were almost completely digested by
258 the sulphuric acid. This is reasonable, since the hemicelluloses are known to act as an
259 amophous matrix interacting with the cellulose microfibrils in plant cell walls (Cosgrove 2012;
260 Dick-Pérez et al. 2011; Martínez-Sanz et al. 2015a). The most remarkable difference between
261 the extracted nanocrystals was the presence of defined peaks located at 2912 and 2845 cm^{-1} in
262 both NANO F3A and NANO F2A spectra. This indicates that some of the lipidic impurities
263 remaining in the F2A and F3A fractions were not completely removed by the acid hydrolysis
264 treatment. The same has been reported to happen during the hydrolysis of *Schizochytrium*
265 *limacinum*, a high lipid content microalgae, for the production of biodiesel (Johnson and Wen

2009). This may be due to either an inherent crystalline structure of the lipidic impurities or to strong interactions existing between these components and the cellulose microfibrils. In the latter case, the acid would have digested preferentially those components such as hemicelluloses which were more accessible. This seems to be the most plausible explanation, since no additional peaks arising from the presence of crystalline components, other than cellulose, were detected in the XRD espectra of neither NANO F2A nor NANO F3A (cf. Figure 3).

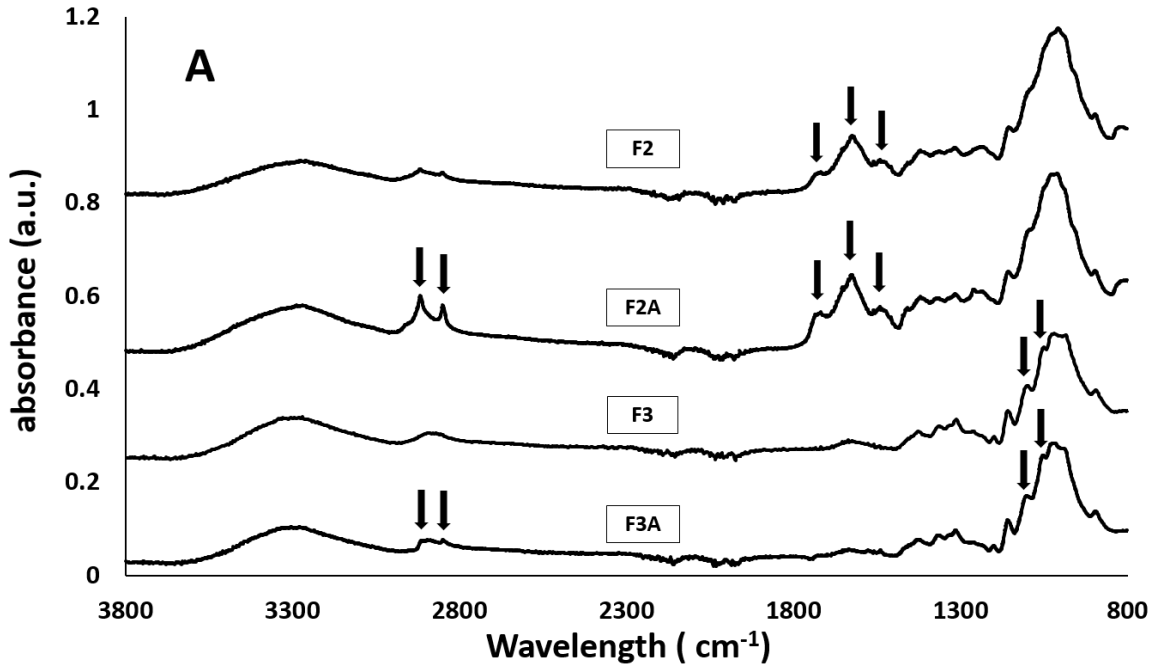

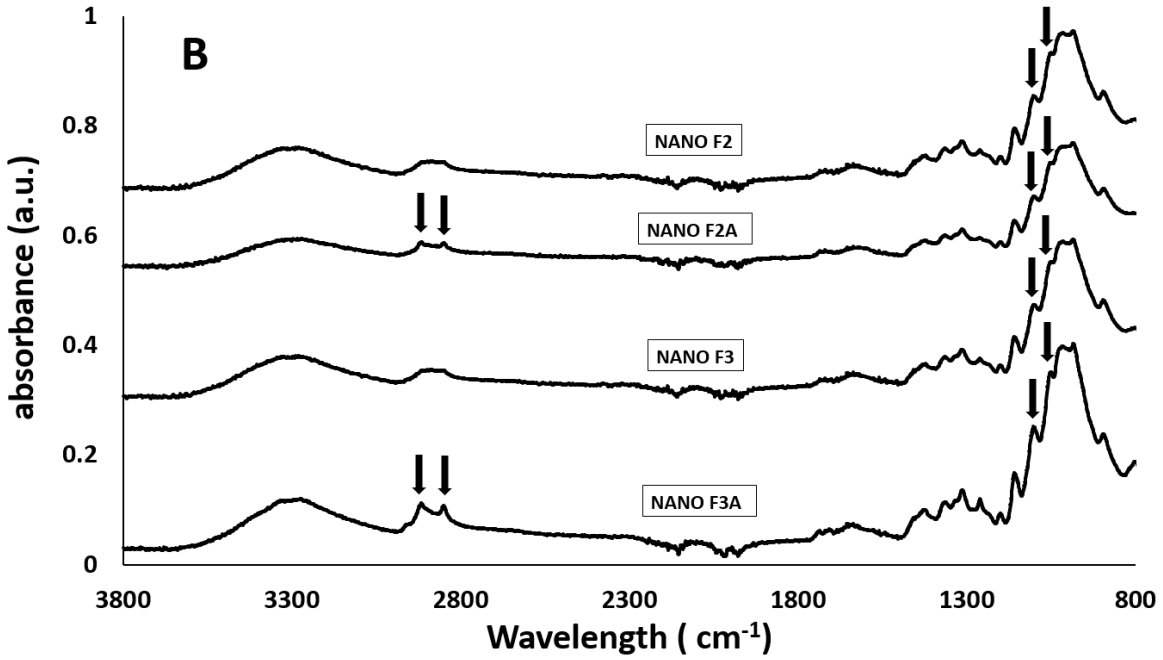

Figure 2. FT-IR spectra of (A) the cellulosic fractions and (B) the extracted nanocrystals. Spectra have been offset for clarity. Arrows point out to the spectral bands displaying the most significant changes amongst the different materials.

XRD analyses were carried out to corroborate the successful purification of the cellulosic fractions and assess the effect of hydrolysis on the crystallinity of the extracted nanocrystals. As observed in Figure 3, all the samples presented very similar spectra, composed of three peaks located at 15.0, 16.6 and 22.7º, which correspond to the (1-10), (110) and (200) crystalline planes from the cellulose Iβ crystalline allomorph (Gupta et al. 2016; Thomas et al. 2013; Wada et al. 1993). Crystallinity indexes and crystallite sizes were calculated by fitting the experimental data and the results are summarized in Table 1. When comparing between the cellulosic fractions, F3 (i.e. pure cellulose) had the highest crystallinity index (66.9%), similar to that previously reported for the cellulose extracted from *Posidonia oceanica* (Benito-González et al. 2018). The presence of amorphous hemicelluloses and other impurities in the rest of the fractions led to reduced crystallinity values in the obtained films. A significant increase in the crystallinity after the acid hydrolysis treatment was observed for all the

fractions, although this effect was less pronounced for the F2A and F3A fractions. This suggests that the presence of lipidic impurities in these fractions hindered the accessibility of the acid to digest the amorphous hemicelluloses and the defective regions in the cellulose microfibrils. The heterogeneity in the effect observed in the crystallite sizes precludes from drawing any conclusions but, in general, it seems that the overall crystallite sizes remained unaffected, confirming that the acid digested preferentially amorphous matrix components such as hemicelluloses rather than cellulose amorphous/paracrystalline domains. The NANO F3 sample presented a relatively high crystallinity index of ca. 76.5%, which is greater than those previously reported for nanocrystals extracted from *Gelidiella aceroso* (Singh et al. 2017) or garlic straw (Kallel et al. 2016), and very similar to those obtained from *Gelidium elegans* (Chen et al. 2016), *Pennisetum sinese* (Lu et al. 2014) and bacterial cellulose nanocrystals obtained in similar reaction times (Martínez-Sanz et al. 2011).

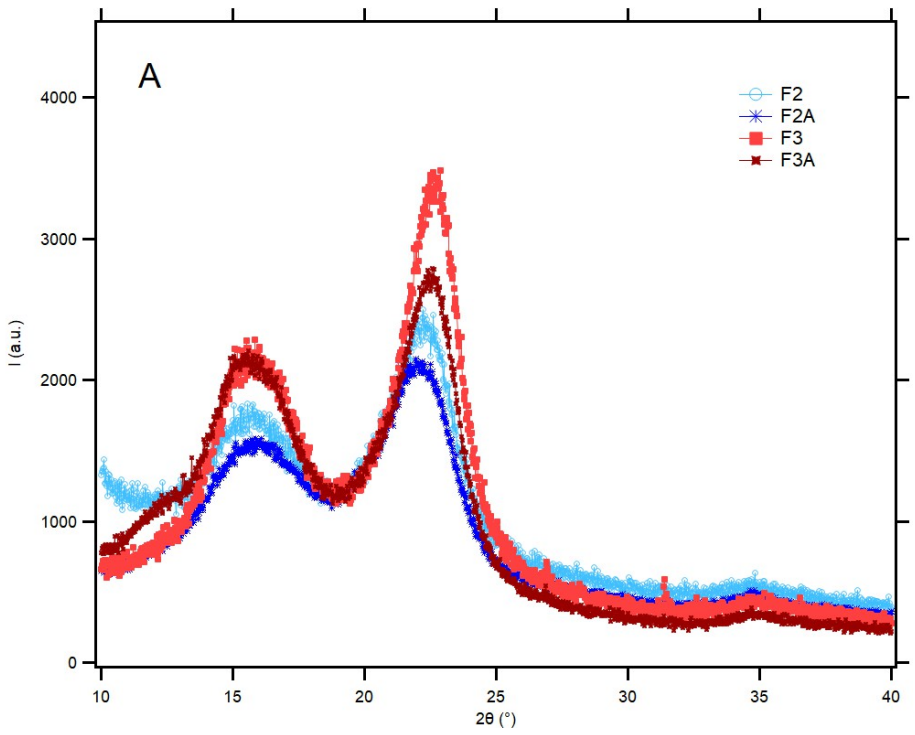

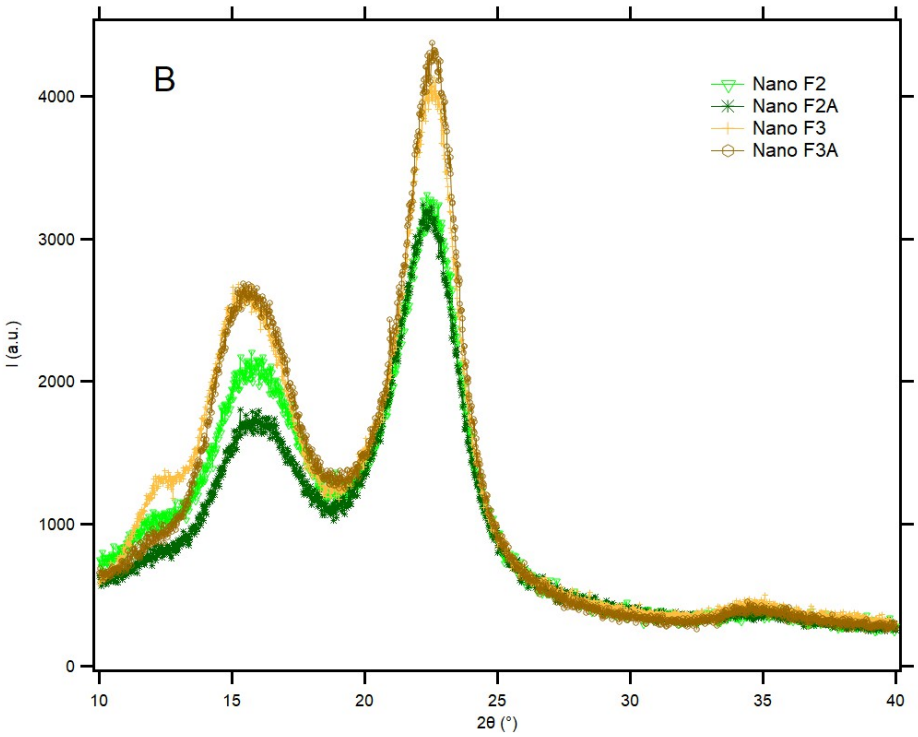

306

307 **Figure 3.** XRD patterns of (A) the cellulosic fractions and (B) the extracted nanocrystals.

308

309 **Table 1.** Crystallinity index (X_C) and cross-sectional dimensions of crystallite sizes in the
310 direction perpendicular to the (1-10), (110) and (200) planes ($D_{(1-10)}$, $D_{(110)}$ and $D_{(200)}$),
311 determined from the XRD patterns.

	X_C (%)	$D_{1\text{-}10}$ (nm)	D_{110} (nm)	D_{200} (nm)
F2	44.1	4.5	3.5	3.5
F2A	48.0	3.4	5.5	3.3
F3	66.9	2.9	6.5	3.7
F3A	54.8	4.1	4.2	3.8
NANO F2	55.8	3.2	5.5	3.5
NANO F2A	50.0	3.4	5.3	3.4
NANO F3	76.5	3.1	5.3	3.6
NANO F3A	62.2	3.3	5.5	3.8

312

313 The rigid cellulose components (i.e. those components with reduced mobility) in the extracted
314 nanocrystals were examined using solid-state ^{13}C CP/MAS NMR and the spectra obtained are
315 shown in Figure 4. The characteristic peaks of cellulose, which correspond to the different
316 carbons in the cellulose structure as highlighted, were present in the four samples. As observed,
317 the peak shape and position was different for the NANO F2-NANO F2A and the NANO F3-
318 NANO F3A samples. The broader and less intense peaks detected in the NANO F2 and NANO
319 F2A samples are indicative of the presence of hemicelluloses. The cellulose crystallinity index
320 was estimated by integration of the signals at 85-92 ppm and at 80-85 ppm, corresponding to
321 the C-4 carbons from the crystalline and non-crystalline cellulose regions, respectively (Foston,
322 2014). The calculated crystallinity values, ca. 42% for NANO F2, 36% for NANO F2A, 46%
323 for NANO F3 and 39% for NANO F3A, were much lower than those estimated from the XRD
324 results. A similar discrepancy between XRD and NMR has been reported for cellulose samples
325 from diverse sources (Chen et al. 2017; Martínez-Sanz et al. 2016; Martinez-Sanz et al. 2017;
326 Park et al. 2009) and has been explained by the different ability of these techniques to
327 distinguish between crystalline and paracrystalline domains. While the contribution from both
328 the crystalline and paracrystalline fractions is accounted for in the XRD-calculated
329 crystallinity, the NMR technique is able to differentiate the crystalline versus the
330 paracrystalline domains since the carbons located within the interior crystalline regions have a
331 chemical shift distinct from those carbons located on the crystallite surfaces or paracrystalline
332 domains (Oehme et al. 2015). According to that, the NANO F2 and NANO F2A would be the
333 samples with the highest amorphous cellulose content, while the NANO F3 and NANO F3A
334 would present the greatest paracrystalline fractions. This provides further evidence for the
335 presence of amorphous hemicelluloses tightly bound to the cellulose microfibrils, which
336 remain in the less purified fractions even after the hydrolysis process. Furthermore, it should
337 also be noted that a small peak located at ca. 33.4 ppm was detected in the NANO F2A and

NANO F3A fractions. This peak has been previously assigned to the presence of lipids in cellulose-derived samples (Kikuchi et al. 2000; Wang et al. 2015; Yamazawa et al. 2013) and therefore, it supports the presence of a certain lipidic fraction in the nanocrystals obtained from the fractions which were not subjected to the Soxhlet treatment.

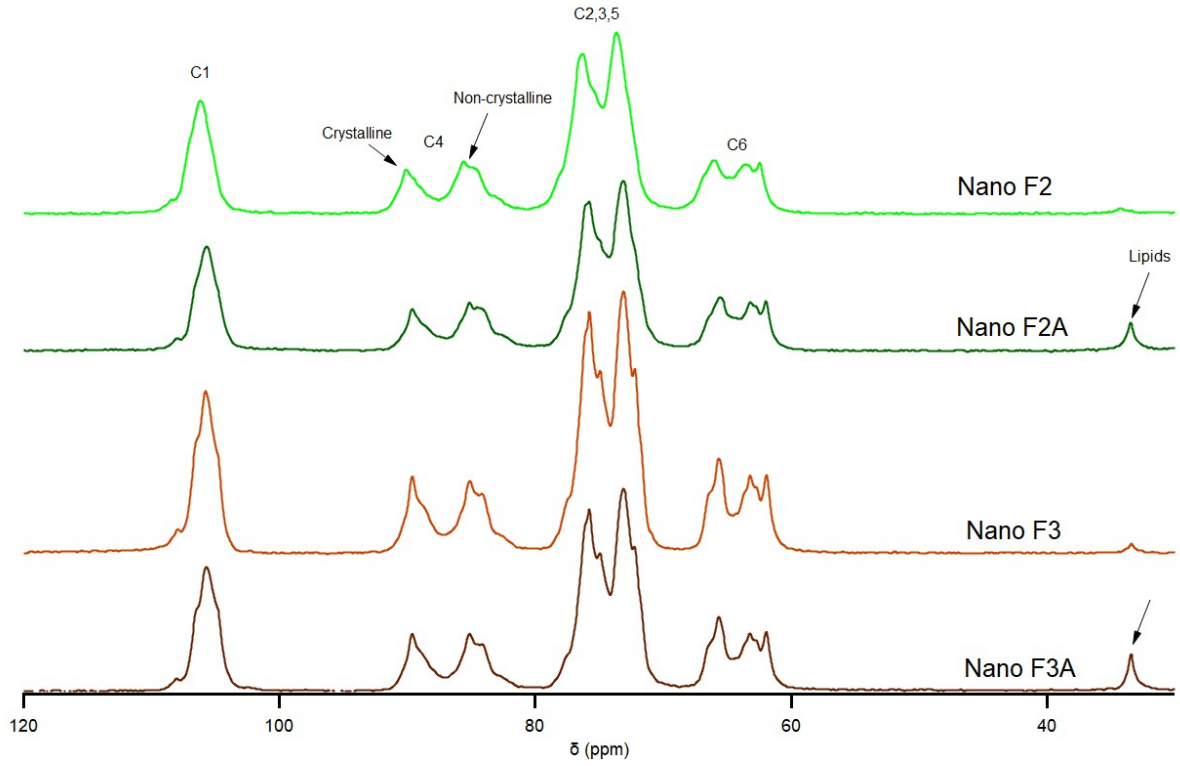

Figure 4. NMR patterns of the different nanocrystals obtained. Carbons 1-6, crystalline and non-crystalline regions and lipid peaks are pointed by an arrow.

The morphology of the extracted nanocrystals was evaluated by TEM and representative images are shown in Figure 5. The material extracted from F3 (pure cellulose) presented a very similar morphology to that of cellulose nanocrystals previously extracted by the sulphuric acid hydrolysis protocol used in this work (Martínez-Sanz et al. 2011; Martínez-Sanz et al. 2015b). This type of nanostructures are often designated as cellulose nanowhiskers due to their needle-

like morphology. On the other hand, the nanocrystals obtained from the non-purified fractions clearly contained some impurities. Interestingly, a greater degree of agglomeration was observed for the NANO F2 and NANO F2A samples. This might be due to the presence of very limited amounts of hemicelluloses, which were resistant to the acid hydrolsysis. In fact, it has been previously reported that minor fractions of hemicelluloses are intimately interacting with the cellulose microfibrils in plant cell walls (Martínez-Sanz et al. 2015a) and can only be removed by using specific enzymes (Pauly et al. 1999). In the case of NANO F3A and NANO F2A, some impurities, which were stained providing higher contrast than the cellulose nanocrystals, were identified. This is indicative of the presence of compounds attached to the surface of the nanocrystals, which had higher affinity for the uranile acetate dye, such as fatty acids and pigments. Despite the presence of impurities in some of the samples, all the extracted nanocrystals had very similar dimensions (cf. Table 2), with lenghts ranging from ca. 488 nm to 586 nm and widths between ca. 10 nm to 15 nm, which were comparable to those reported for cellulose nanocrystals obtained from bacterial cellulose (Martínez-Sanz et al. 2011) and slightly larger than cotton cellulose nanocrystals (Lagerwall et al. 2014). The large aspect ratios of the extracted nanocrystals, greater than 30, highlight the potential of those materials for being used as reinforcing materials in polymeric composites.

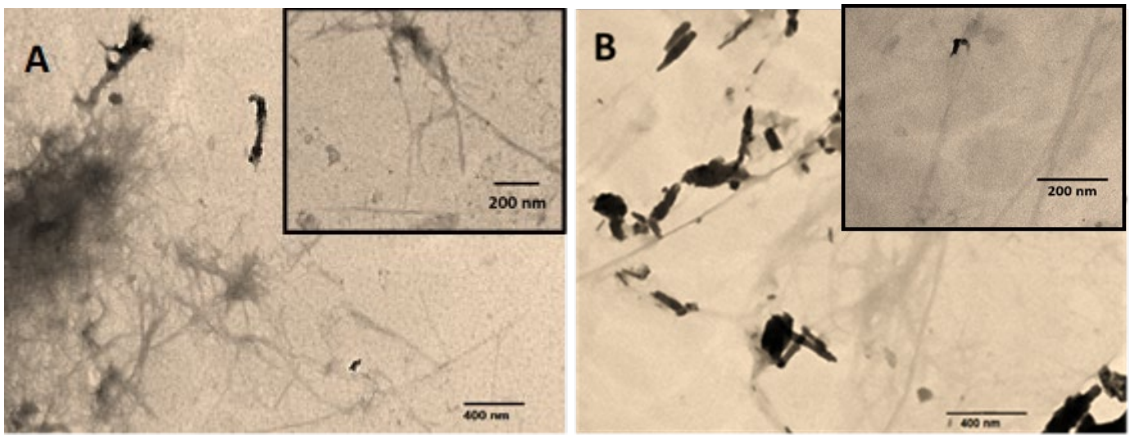

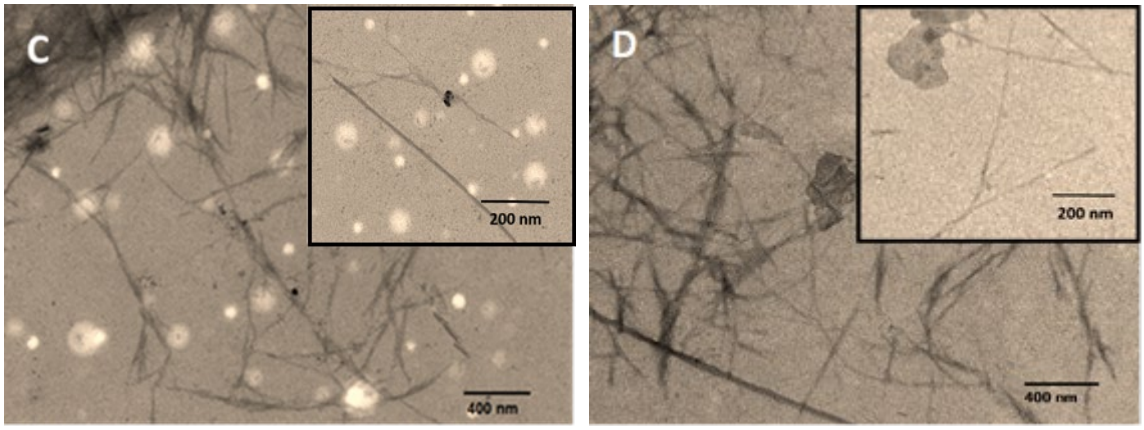

Figure 5. Representative TEM images of the extracted nanocrystals: (A) NANO F2, (B) NANO F2A, (C) NANO F3 and (D) NANO F3A. Inserts correspond to higher magnification images.

Table 2. Size (width and length) and aspect ratio of the extracted nanocrystals.

	Width (nm)	Length (nm)	Aspect ratio
NANO F2	10.7 ± 2.8[a]	487.5 ± 86.3[a]	45.6
NANO F2A	14.9 ± 4.7[a]	499.0 ± 96.1[a]	33.5
NANO F3	10.8 ± 2.2[a]	514.0 ± 82.5[a]	47.6
NANO F3A	10.1 ± 3.3[a]	586.4 ± 103.4[a]	58.1

3.2. Characterization of the cellulosic films

The different cellulosic fractions and the extracted nanocrystals were used to generate cellulosic films by means of a simple vacuum filtration method using aqueous dispersions. The surface morphology of the obtained films was evaluated by SEM and representative images are displayed in Figure 6. On the one hand, a lower magnification was used to observe the general structure of the cellulosic films (scale bars corresponding to 1 mm), evidencing a clearly higher porosity in both the F2 and F2A films (where even different layers of fibres

386 could be easily appreciated) in comparison with the F3 and F3A films. The latter ones presented
387 much smoother surfaces, with the cellulose fibres being clearly identified in the F3 film. The
388 F3A film presented a much more compact structure, most likely caused by the presence of
389 lipidic compounds which formed a coating layer on the surface of the film. On the other hand,
390 the structure of the films produced from the nanocrystals were compared at a higher
391 magnification (scale bars corresponding to 100 μm) since all the samples appeared identical,
392 with very smooth surfaces, at the lower magnification used for the cellulosic films. As
393 observed, all the films showed a very compact structure with no significant differences between
394 them.

395

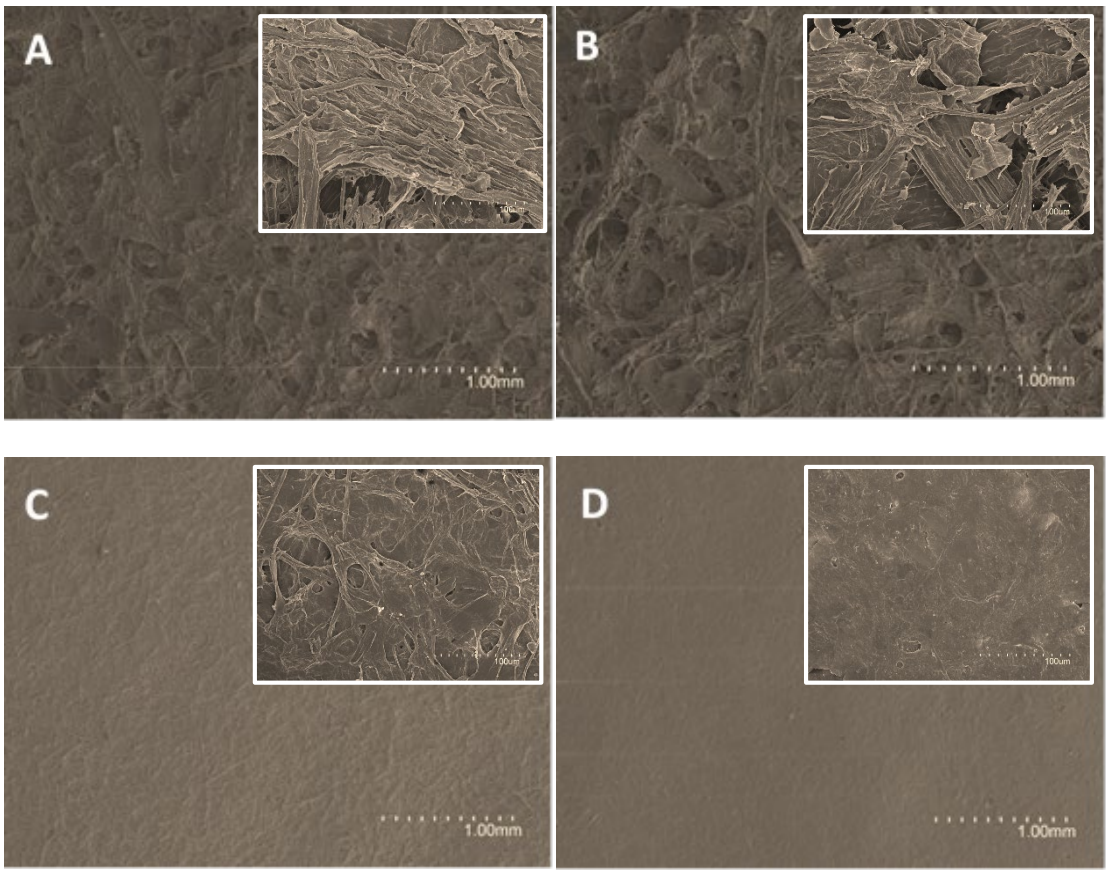

396

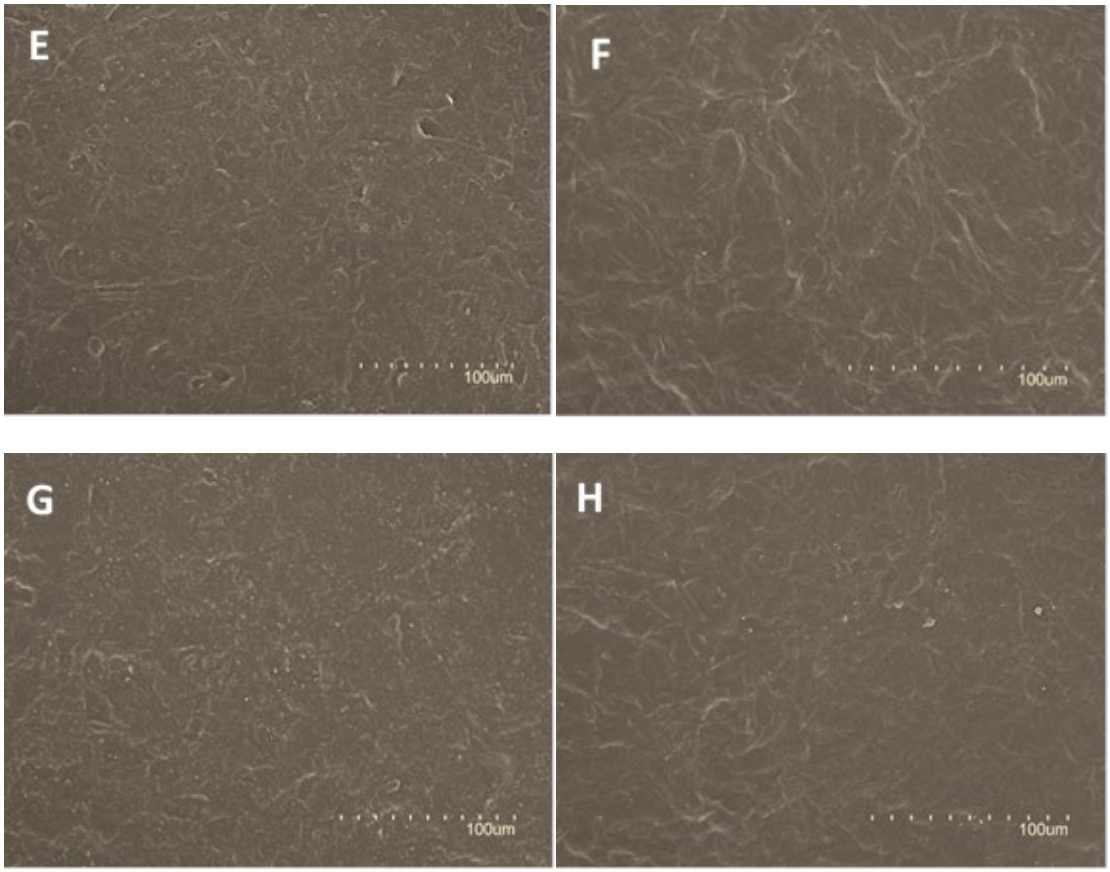

Figure 6. SEM images of the surface from the cellulosic films: (A) F2, (B) F2A, (C) F3 and (D) F3A, (E) NANO F2, (F) NANO F2A, (G) NANO F3 and (H) NANO F3A. Inserts in A-D correspond to higher magnification images.

Since these films were intended to be used in food packaging applications, transparency was an important attribute to be evaluated. Figure 7A shows the visual appearance of the different films. It can be clearly observed that while the films obtained from the fractions were completely opaque (F2, F2A and F3A) with a white tonality, or translucent (F3), all the films produced from the nanocrystals were transparent. Therefore, while in the case of the fractions, the most purified ones were more transparent, the acid hydrolysis tended to equalize transparency with a substantial increase of it in all cases. The transparency of the films was quantitatively assessed by measuring their internal transmittance, as shown in Figure 7B. As observed, all the films obtained from the cellulosic fractions, except the F3 film, displayed low

412 transmittance values (i.e. low transparency) since they had a translucid appearance with a
413 strong white tonality. The greater transparency of the F3 film may be due to the better
414 dispersion of the cellulose fibers in this particular sample, giving rise to films with more
415 homogenous surfaces, as suggested by SEM (cf. Figure 5C). As expected, the films prepared
416 from the nanocrystals showed much higher transparency due to the decreased particle size
417 produced after the acid hydrolysis treatment. No significant differences were found between
418 the four nanocrystal films, which displayed similar results to those of corn starch films (Benito-
419 González et al. 2018).
420

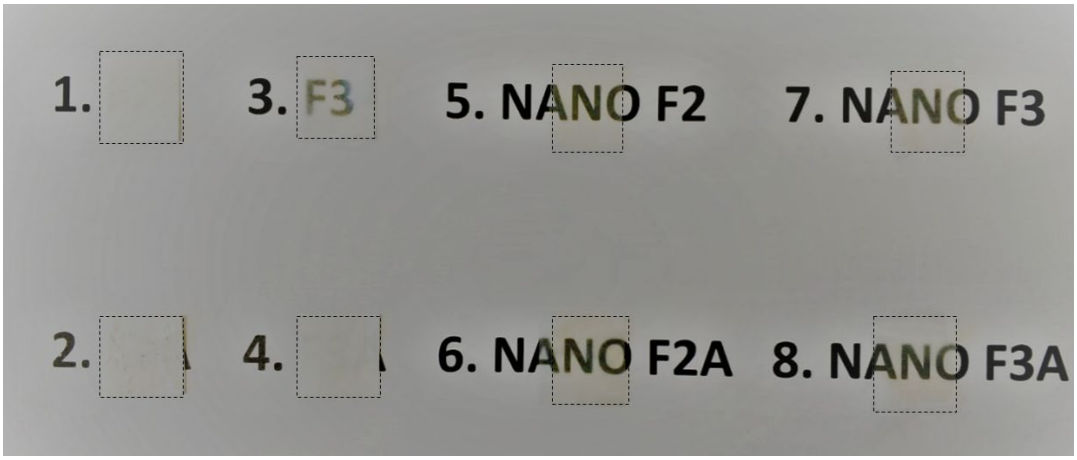

421

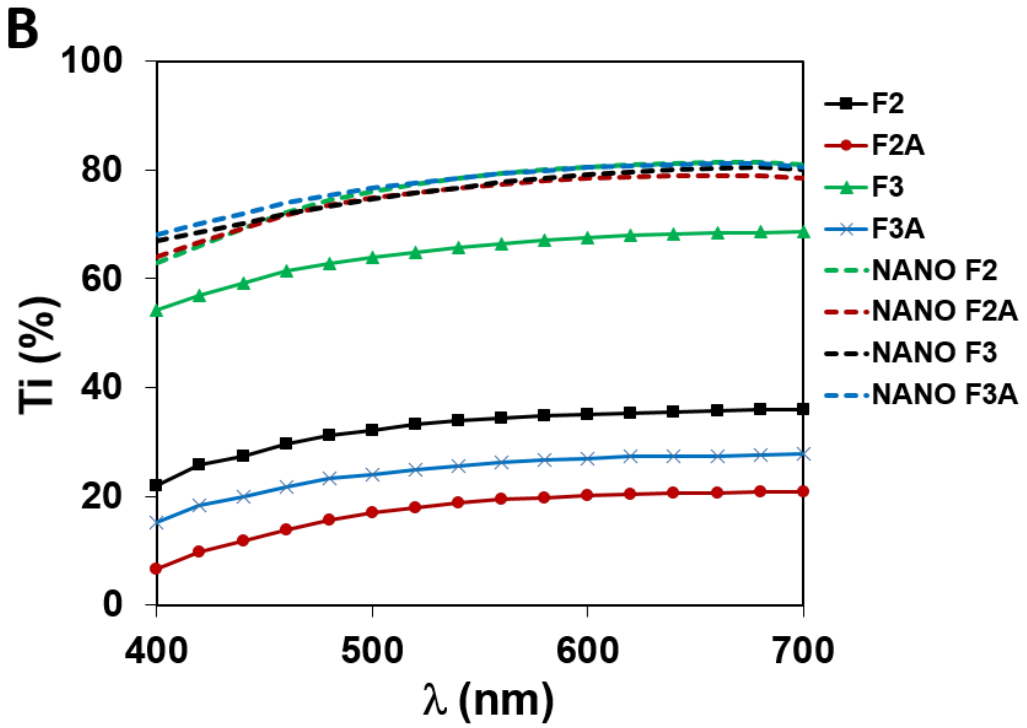

Figure 7. (A) Visual appearance and (B) spectral distribution of internal transmittance (Ti) of the different cellulosic fractions and nanocrystals obtained.

The mechanical properties of the films from the cellulosic fractions and the extracted nanocrystals were evaluated, and the results are summarized in Table 3. When comparing the films from the cellulosic fractions, the first clear observation was that the removal of hemicelluloses had a great impact in the mechanical performance of the films, as the F3 and F3A films presented significantly greater elastic modulus, tensile strength and elongation at break than the F2 and F2A films. The improved mechanical performance of pure cellulose films has been previously reported (Benito-González et al. 2018) and ascribed to an easier dispersion of cellulose in water when hemicelluloses are removed, hence producing more homogeneous aqueous dispersions for the production of films. Additionally, the presence of lipidic impurities when omitting the initial Soxhlet treatment had a negative impact in the mechanical properties, reducing the stiffness of the material (F3 presented higher elastic

437 modulus and tensile strength than F3A). Thus, the pure cellulose film would be the optimum
438 in terms of mechanical performance.

439 The acid hydrolysis of the different fractions had a strong positive effect on the mechanical
440 properties of the produced films. This was much more evident for the F2 and F2A fractions,
441 with ca. 30-fold increase in the tensile strength and more than 10-fold increase in the elastic
442 modulus. While the elongation at break increased after hydrolyzing the F2 and F2A fractions,
443 it slightly decreased in the case of the F3 and F3A fractions. These results suggest that the acid
444 hydrolysis was able to digest some of the amorphous hemicelluloses present in the F2 and F2A
445 fractions, leading to a favorable effect in the mechanical properties of the NANO F2 and
446 NANO F2A films. On the other hand, in the case of the F3 and F3A fractions, the hydrolysis
447 process resulted in the digestion of the cellulose amorphous/paracrystalline domains, yielding
448 more rigid crystalline structures. Surprisingly, although there were no significant differences
449 in the elastic modulus of the films prepared from the nanocrystals, the tensile strength and
450 elongation at break were substantially higher in NANO F2 and NANO F2A as compared with
451 NANO F3 and NANO F3A. It has been demonstrated that in plant cell walls, a certain fraction
452 of hemicelluloses intimately interacts with cellulose microfibrils (Martínez-Sanz et al. 2015a),
453 having a very limited accessibility and only being removed by the action of specific enzymes
454 (Pauly et al. 1999). Therefore, it is reasonable to hypothesize that a certain fraction of
455 hemicelluloses, strongly interacting with the cellulose microfibrils, remained in the material
456 even after the acid hydrolysis. The presence of these hemicelluloses improved the strength and
457 ductility of the films, which is in agreement with previous studies that demonstrated the crucial
458 role of some hemicelluloses, such as xyloglucan and mannans, in the micromechanics of plant
459 cell walls and cellulose hydrogels (Lopez-Sanchez et al. 2015; Whitney et al. 1998). The films
460 obtained from the nanocrystals extracted from F2A and F3A (i.e. avoiding the Soxhlet
461 extraction) presented similar properties to those obtained from the F2 and F3 nanocrystals, with

462 only a slight reduction in the tensile strength. This implies that it is possible to obtain materials
463 with very similar mechanical properties with less purification steps (i.e. reducing the
464 processing time and the associated costs and avoiding the use of organic solvents).

465 It is worth noting that all the films prepared from the extracted nanocrystals displayed excellent
466 mechanical performance, showing higher elastic modulus, tensile strength and elongation at
467 break than films from bacterial cellulose nanocrystals (BCNW) (Martínez-Sanz et al. 2013)
468 and microfibrillated cellulose (MFC) (Plackett et al. 2010). The greater elastic modulus and
469 tensile strength of the NANO F3 film as compared with BCNW is surprising considering the
470 significantly higher crystallinity index previously reported for BCNW (Xc~95%) (Martínez-
471 Sanz et al. 2013). One possible explanation for the improved mechanical performance of the
472 *Posidonia oceanica* nanocrystals is related to their greater aspect ratio (ca. 48 for NANO F3
473 versus 30 for BCNW (Martínez-Sanz et al. 2013)). Furthermore, the film density and relative
474 humidity at which the films are conditioned prior to the mechanical testing have been reported
475 to have an impact in the mechanical performance of the films (Reising et al. 2012). It is possible
476 that the low relative humidity used for the pre-conditioning of the *Posidonia* nanocrystals films
477 (0% RH) may be also responsible for their stiffer behavior. When comparing with benchmark
478 biopolymers such as thermoplastic corn starch (TPCS) (Fabra et al. 2016) and PLA (Mathew
479 et al. 2005), all the nanocrystal films showed an obvious improvement in terms of Young's
480 modulus and tensile strength, making these films a promising alternative for food packaging.
481 The results were even comparable to those from petroleum-based polymers widely used in food
482 packaging applications, such as polyethylene terephthalate (PET) and oriented polystyrene
483 (OPS) (Auras et al. 2005) and in particular, the nanocrystal films were superior to these
484 materials in terms of stiffness.
485

Table 3. Mechanical properties (Young's modulus, tensile strength and elongation at break) from the films obtained from cellulosic fractions and nanocrystals.

	E (GPa)	Tensile Strength (MPa)	ε_b (%)
F2	0.8 ± 0.1^{a}	4.6 ± 0.1^{a}	1.1 ± 0.3^{ab}
F2A	1.0 ± 0.1^{a}	4.8 ± 0.6^{a}	0.7 ± 0.1^{a}
F3	4.2 ± 0.4^{c}	45.9 ± 6.9^{c}	2.1 ± 0.4^{c}
F3A	2.6 ± 0.4^{b}	22.1 ± 1.8^{b}	1.6 ± 0.3^{bc}
NANO F2	11.5 ± 0.8^{d}	142.0 ± 4.3^{g}	2.8 ± 0.2^{d}
NANO F2A	10.5 ± 1.4^{d}	124.7 ± 7.2^{f}	2.4 ± 0.4^{cd}
NANO F3	11.5 ± 1.1^{d}	98.0 ± 6.8^{e}	1.1 ± 0.3^{ab}
NANO F3A	12.2 ± 0.5^{d}	72.1 ± 3.7^{d}	1.2 ± 0.1^{b}
BCNW (Martínez-Sanz et al. 2013)	7.9 ± 0.1	74.6 ± 11.5	1.0 ± 0.1
MCF (Plackett et al. 2010)	2.1 ± 0.1	39.0 ± 8.0	2.8 ± 0.9
PLA (Martínez-Sanz et al. 2012; Mathew et al. 2005)	(1.9-3.6) ± (0.1-0.2)	(49.6-53.8) ± (1.0-1.2)	(2.4-4.9) ± (0.1-0.5)
TPCS (Fabra et al. 2016)	0.1 ± 0.0	11.2 ± 0.8	7.3 ± 1.9

PET (Auras et al. 2005)	~ 1.6	~ 55.1	~ 4.2
OPS (Auras et al. 2005)	~ 1.6	~ 58.6	~ 4.3

The water vapour permeability (WVP) of the different films was also measured and the results are shown in Table 4. When comparing the films from the cellulosic fractions, the F3 film was clearly the optimum. Similarly to the mechanical properties, the water vapour barrier effect was improved by removing most of the hemicelluloses. Furthermore, the presence of lipids when eliminating the Soxhlet step did not have a positive impact in the water permeability of the films. As deduced from the results, the films obtained from the nanocrystals displayed remarkably lower water permeability (an order of magnitude lower than those of the films from their respective fractions). This is most likely due to the increased crystallinity of the materials after the hydrolysis and the more compacted film structure, as evidenced by SEM. Amongst them, NANO F2 was clearly the least impermeable film, while NANO F2A presented the highest barrier possibly due to the lipidic presence as reported by other authors (Galus and Kadzińska 2016; Sánchez-González et al. 2009). From the results, it seems that the removal of hydrophilic compounds such as the hemicelluloses gave rise to a reduced permeability, while the presence of hydrophobic impurities such as those removed by the Soxhlet treatment had a positive effect.

The water permeability values from all the nanocrystal films were similar or even slightly better than those previously reported for films from BCNW (Martínez-Sanz et al. 2013) and from MFC (Rodionova et al. 2011). All the cellulosic fractions and nanocrystals outperformed TPCS in terms of water vapour barrier (Fabra et al. 2016), while only the NANO F2A film was comparable to more hydrophobic biopolymers such as PLA (Martínez-Sanz et al. 2012). However, all the developed films were still far from reaching comparable water vapour barrier values to those from highly hydrophobic petroleum-based polymers such as PET and OPS

511 (Auras et al. 2005). The improvement in the water barrier performance originated by the
512 presence of the impurities remaining in the NANO F2A and NANO F3A, mostly lipids as
513 suggested by the FTIR results, is an interesting result since it implies the possibility of
514 obtaining materials with excellent barrier performance using a greener and simpler extraction
515 protocol.
516 Water uptake measurements are also compiled in Table 4. From all the cellulosic fractions, the
517 pure cellulose (i.e. F3) presented the lowest water sorption capacity. This is related to the lower
518 water accessibility towards the more crystalline structure of F3. The presence of fatty acids
519 remaining in the F2A fraction seemed to promote a more hydrophobic behavior as compared
520 with F2, thus reducing the water uptake. This effect was not observed for F3A most likely due
521 to its lower crystallinity when compared with F3. On the other hand, water uptake results for
522 the nanocrystals were consistent with results displayed in Table 1. As the crystallinity index
523 increased, a more hydrophobic behavior was shown by the surface, being F3 the material with
524 lower water sorption values. The fact that there were no significant differences between the
525 cellulosic fractions and the nanocrystals might be explained by means of thickness, as the ratio
526 surface exposure/total weight was much higher in the case of nanocrystals. Furthermore,
527 contact angle measurements were carried out to confirm the water affinity of the surface from
528 the different films. Due to their highly hydrophilic behavior, the F2, F2A and F3A films could
529 not be tested since they absorbed the water drop as soon as it was deposited on top of the film
530 surface. Interestingly, the F3 film presented a much more hydrophobic behavior, which may
531 be explained by the greater crystallinity of the pure cellulose as opposed to the less purified
532 fractions. Furthermore, although cellulose is known to contain a large amount of hydroxyl
533 groups, the cellulose microfibrils tend to self-associate through the formation of strong
534 hydrogen bonds and as a result, most of these hydrophilic groups are not available to interact
535 with water. The sulphuric acid treatment clearly promoted a more hydrophobic behavior of the

536 films' surface by removing hydrophilic hemicelluloses and amorphous cellulose. The most
537 hydrophobic surface was that from the NANO F3 film, which was not surprising due to the
538 higher crystallinity of this material and the strong self-association of pure cellulose when
539 impurities were absent. The presence of hemicelluloses, even at very limited amounts, yielded
540 more hydrophilic surfaces due to the presence of free hydroxyl groups. Surprisingly, the lipidic
541 impurities remaining in the NANO F2A and NANO F3A films led to more hydrophilic
542 surfaces. This might be due to the disruption of the cellulose hydrogen bonding network caused
543 by the presence of impurities, hence increasing the amount of free hydroxyl groups available
544 to interact with water. This indicates that the reduced water vapour permeability induced by
545 the presence of lipidic impurities was mostly caused by a reduction in the water diffusion
546 through the films.
547 Oxygen permeability of the films was also determined and results are shown in Table 4. Lipids
548 seemed to have a clear disrupting effect as the films produced from the nanocrystals obtained
549 without Soxhlet treatment presented higher values when compared with those obtained from
550 the more purified fractions (up to 30 times). Similar results have been previously obtained for
551 films loaded with essential oils (Galus and Kadzińska 2016; Ghasemlou et al. 2013). On the
552 other hand, both NANO F2 and NANO F3 displayed outstanding values similar to PLA
553 (Martínez-Sanz et al. 2012) demonstrating the potential of the fraction containing
554 hemicelluloses for developing biodegradable packaging materials reducing associated costs.
555
556 **Table 4.** Water vapour permeability, water uptake, contact angle and oxigen permeability of
557 the films obtained from the cellulosic fractions and nanocrystals.

	WVP·10^{13} (kg·m/s·m^2·Pa)	**Water uptake (%)**	**Contact angle (º)**	**OP·10^{18} (m^3·m/Pa·s·m^2)**
F2	35.2 ± 0.6[a]	18.0 ± 3.1[a]	n.m.	n.m.

F2A	34.4 ± 2.2[a]	20.8 ± 1.7[a]	n.m.	n.m.
F3	12.5 ± 3.3[c]	6.8 ± 2.3[c]	80.0 ± 2.8[b]	311.4 ± 10.2[e]
F3A	22.2 ± 2.7[b]	13.1 ± 0.7[b]	n.m.	n.m.
NANO F2	4.8 ± 0.4[d]	17.7 ± 3.1[a]	77.4 ± 7.1[ab]	2.0 ± 0.4[b]
NANO F2A	1.8 ± 0.1[f]	20.2 ± 0.9[a]	68.3 ± 2.9[a]	60.7 ± 6.9[d]
NANO F3	2.7 ± 0.4[e]	10.5 ± 1.8[bc]	102.1 ± 3.9[c]	1.1 ± 0.1[a]
NANO F3A	2.2 ± 0.2[ef]	13.8 ± 0.9[b]	76.4 ± 8.0[ab]	22.9 ± 0.4[c]
BCNW (Martínez-Sanz et al. 2013)	3.6 ± 1.1	5.0 ± 0.7	43.8 ± 1.0	6.0
MFC (Plackett et al. 2010)	3.8	---	---	22
PLA (Martínez-Sanz et al. 2012)	1.3 ± 0.1	1.0 ± 0.1	---	1.8
TPCS (Fabra et al. 2016)	15.5 ± 0.1	---	10.5 ± 2.1	41.0 ± 2.3
PET (Auras et al. 2005; Polyakova et al. 2001)	0.03 ± 0.0002	---	---	0.3 ± 0.02
OPS (Auras et al. 2005)	0.04 ± 0.0002	---	---	---

n.m.: Not measurable.

4. Conclusions

The waste biomass from *Posidonia oceanica* leaves has been valorized to extract cellulosic fractions with distinct composition by exploring different extraction protocols. The presence of hemicelluloses in the F2 and F2A fractions was confirmed and it was seen to reduce the overall crystallinity of the fractions. On the other hand, omitting the Soxhlet treatment led to the presence of lipidic impurities in the F2A and F3A fractions, which were also detrimental in terms of crystallinity. Additionally, these fractions were subjected to an acid hydrolysis

567 treatment to digest the amorphous domains of the material, yielding cellulosic nanocrystals
568 with aspect ratios higher than 30. Although the amorphous hemicelluloses were preferentially
569 digested by the acid, a small fraction seemed to remain in NANO F2 and NANO F2A. Lipids
570 were also somehow resistant to the hydrolysis and hindered to some extent the access of
571 sulphuric acid towards the cellulose amorphous domains. The pure cellulose nanocrystals
572 showed the most optimal properties, with an aspect ratio of ca. 48 and crystallinity of ca. 77%.
573 Aqueous suspensions from all these fractions and nanocrystals were used to generate films by
574 a simple vacuum filtration method. For the films produced from the fractions, cellulose
575 purification led to a major improvement in the visual appearance, mechanical performance and
576 barrier properties. Moreover, the acid hydrolysis of the amorphous components in the fractions
577 had a strong positive impact in the properties of the films, especially in the case of the less
578 purified fractions, yielding films with superior mechanical properties to that of benchmark
579 biopolymers and barrier properties comparable even to that of more hydrophobic biopolymers
580 such as PLA. The presence of lipids in the nanocrystals had a limited effect in the mechanical
581 properties but was seen to induce a decrease in the water vapor permeability by hindering the
582 diffusion of water molecules through the films, while oxygen permeability was negatively
583 affected. On the other hand, the presence of a minor fraction of hemicelluloses, strongly
584 interacting with the cellulose nanocrystals, showed a high positive impact on the mechanical
585 performance but led to decreased water barrier due to the more hydrophilic character of the
586 material. Overall, the less purified hemicellulose-containing NANO F2 and NANO F2A films
587 were the optimum materials, offering a good compromise in terms of mechanical and barrier
588 performance, while reducing the amount of purification steps and, in the case of F2A, avoiding
589 the use of organic solvents.
590 These results show the enormous potential of *Posidonia oceanica* waste biomass to produce
591 less purified cellulose-based nanocrystals by applying simpler and greener extraction protocols

592 and develop high-performance films, which outperform many benchmark biopolymers,
593 valuable for food packaging applications.
594

595 ## Acknowledgements

596 This work was financially supported by the project GV/2018//149, the "Agencia Estatal de
597 Investigación" and co-funded by the European Union's Horizon 2020 research and innovation
598 programme (ERA-Net SUSFOOD2). Marta Martínez-Sanz is recipient of a Juan de la Cierva
599 (IJCI-2015-23389) contract from the Spanish Ministry of Economy, Industry and
600 Competitiveness.
601

602 ## Disclosure

603 IBG, MMS and ALR have authored a patent on the extraction protocol to produce cellulose-
604 based nanocrystals with improved properties.
605

606 ## References

607 Abidi N, Cabrales L, Haigler CH (2014) Changes in the cell wall and cellulose content of developing
608 cotton fibers investigated by FTIR spectroscopy Carbohydrate Polymers 100:9-16
609 Arrieta MP, Fortunati E, Dominici F, Rayón E, López J, Kenny JM (2014) PLA-PHB/cellulose based
610 films: Mechanical, barrier and disintegration properties Polymer Degradation and Stability
611 107:139-149
612 Auras RA, Singh SP, Singh JJ (2005) Evaluation of oriented poly (lactide) polymers vs. existing PET and
613 oriented PS for fresh food service containers Packaging Technology and Science: An
614 International Journal 18:207-216
615 Balata G, Tola A (2017) Cost-opportunity analysis of the use of Posidonia oceanica as a source of bio-
616 energy in tourism-oriented territories. The case of Alghero Journal of Cleaner Production
617 Benito-González I, López-Rubio A, Martínez-Sanz M (2018) Potential of lignocellulosic fractions from
618 Posidonia oceanica to improve barrier and mechanical properties of bio-based packaging
619 materials International Journal of Biological Macromolecules 118:542-551
620 Benito-González I, López-Rubio A, Martínez-Sanz M (2019) HIGH-PERFORMANCE STARCH
621 BIOCOMPOSITES WITH CELULLOSE FROM WASTE BIOMASS: FILM PROPERTIES AND
622 RETROGRADATION BEHAVIOUR Carbohydrate Polymers
623 Bettaieb F, Khiari R, Hassan ML, Belgacem MN, Bras J, Dufresne A, Mhenni MF (2015) Preparation
624 and characterization of new cellulose nanocrystals from marine biomass Posidonia oceanica
625 Industrial Crops and Products 72:175-182 doi:10.1016/j.indcrop.2014.12.038

626 Cao X, Chen Y, Chang PR, Stumborg M, Huneault MA (2008) Green composites reinforced with hemp
627 nanocrystals in plasticized starch Journal of Applied Polymer Science 109:3804-3810
628 Cerisuelo JP, Alonso J, Aucejo S, Gavara R, Hernández-Muñoz P (2012) Modifications induced by the
629 addition of a nanoclay in the functional and active properties of an EVOH film containing
630 carvacrol for food packaging Journal of membrane science 423:247-256
631 Cosgrove DC (2012) Comparative structure and biomechanics of plant primary and secondary cell
632 walls Frontiers in plant science 3:204
633 Chen S-Q et al. (2017) Characterisation of bacterial cellulose from diverse Komagataeibacter strains
634 and their application to construct plant cell wall analogues Cellulose 24:1211-1226
635 Chen YW, Lee HV, Juan JC, Phang S-M (2016) Production of new cellulose nanomaterial from red
636 algae marine biomass Gelidium elegans Carbohydrate polymers 151:1210-1219
637 Dick-Pérez M, Zhang Y, Hayes J, Salazar A, Zabotina OA, Hong M (2011) Structure and interactions of
638 plant cell-wall polysaccharides by two-and three-dimensional magic-angle-spinning solid-
639 state NMR Biochemistry 50:989-1000
640 Dufresne A (2006) Comparing the mechanical properties of high performances polymer
641 nanocomposites from biological sources Journal of nanoscience and nanotechnology 6:322-
642 330
643 Fabra MJ, López-Rubio A, Ambrosio-Martín J, Lagaron JM (2016) Improving the barrier properties of
644 thermoplastic corn starch-based films containing bacterial cellulose nanowhiskers by means
645 of PHA electrospun coatings of interest in food packaging Food Hydrocolloids 61:261-268
646 Fortunati E, Luzi F, Puglia D, Petrucci R, Kenny J, Torre L (2015) Processing of PLA nanocomposites
647 with cellulose nanocrystals extracted from Posidonia oceanica waste: Innovative reuse of
648 coastal plant Industrial Crops and Products 67:439-447
649 Freire C, Silvestre A, Neto CP, Belgacem MN, Gandini A (2006) Controlled heterogeneous
650 modification of cellulose fibers with fatty acids: effect of reaction conditions on the extent of
651 esterification and fiber properties Journal of Applied Polymer Science 100:1093-1102
652 Galus S, Kadzińska J (2016) Whey protein edible films modified with almond and walnut oils Food
653 Hydrocolloids 52:78-86
654 Ghasemlou M, Aliheidari N, Fahmi R, Shojaee-Aliabadi S, Keshavarz B, Cran MJ, Khaksar R (2013)
655 Physical, mechanical and barrier properties of corn starch films incorporated with plant
656 essential oils Carbohydrate polymers 98:1117-1126
657 Gupta V, Carrott P, Singh R, Chaudhary M, Kushwaha S (2016) Cellulose: a review as natural,
658 modified and activated carbon adsorbent Bioresource technology 216:1066-1076
659 Johnson MB, Wen Z (2009) Production of biodiesel fuel from the microalga Schizochytrium
660 limacinum by direct transesterification of algal biomass Energy & Fuels 23:5179-5183
661 Kallel F, Bettaieb F, Khiari R, García A, Bras J, Chaabouni SE (2016) Isolation and structural
662 characterization of cellulose nanocrystals extracted from garlic straw residues Industrial
663 crops and products 87:287-296
664 Khiari R, Marrakchi Z, Belgacem MN, Mauret E, Mhenni F (2011) New lignocellulosic fibres-reinforced
665 composite materials: A stepforward in the valorisation of the Posidonia oceanica balls
666 Composites Science and Technology 71:1867-1872
667 Kikuchi J, Williamson MP, Shimada K, Asakura T (2000) Structure and dynamics of photosynthetic
668 membrane-bound proteins in Rhodobacter sphaeroides, studied with solid-state NMR
669 spectroscopy Photosynthesis research 63:259-267
670 Lagerwall JP, Schütz C, Salajkova M, Noh J, Park JH, Scalia G, Bergström L (2014) Cellulose
671 nanocrystal-based materials: from liquid crystal self-assembly and glass formation to
672 multifunctional thin films NPG Asia Materials 6:e80
673 Lizundia E et al. (2016) PLLA-grafted cellulose nanocrystals: Role of the CNC content and grafting on
674 the PLA bionanocomposite film properties Carbohydrate polymers 142:105-113

675 Lopez-Sanchez P, Cersosimo J, Wang D, Flanagan B, Stokes JR, Gidley MJ (2015) Poroelastic
676 mechanical effects of hemicelluloses on cellulosic hydrogels under compression PLoS One
677 10:e0122132
678 Lu P, Hsieh Y-L (2012) Cellulose isolation and core–shell nanostructures of cellulose nanocrystals
679 from chardonnay grape skins Carbohydrate polymers 87:2546-2553
680 Lu Q-l, Tang L-r, Wang S, Huang B, Chen Y-d, Chen X-r (2014) An investigation on the characteristics
681 of cellulose nanocrystals from Pennisetum sinese biomass and bioenergy 70:267-272
682 Martínez-Sanz M, Erboz E, Fontes C, López-Rubio A (2018) Valorization of Arundo donax for the
683 production of high performance lignocellulosic films Carbohydrate Polymers 199:276-285
684 Martínez-Sanz M, Lopez-Rubio A, Lagaron JM (2011) Optimization of the nanofabrication by acid
685 hydrolysis of bacterial cellulose nanowhiskers Carbohydrate Polymers 85:228-236
686 Martínez-Sanz M, Lopez-Rubio A, Lagaron JM (2013) High-barrier coated bacterial cellulose
687 nanowhiskers films with reduced moisture sensitivity Carbohydrate polymers 98:1072-1082
688 Martínez-Sanz M, Lopez-Rubio A, Lagaron JM (2012) Optimization of the dispersion of unmodified
689 bacterial cellulose nanowhiskers into polylactide via melt compounding to significantly
690 enhance barrier and mechanical properties Biomacromolecules 13:3887-3899
691 Martínez-Sanz M, Lopez-Sanchez P, Gidley MJ, Gilbert EP (2015a) Evidence for differential
692 interaction mechanism of plant cell wall matrix polysaccharides in hierarchically-structured
693 bacterial cellulose Cellulose 22:1541-1563
694 Martínez-Sanz M, Mikkelsen D, Flanagan B, Gidley MJ, Gilbert EP (2016) Multi-scale model for the
695 hierarchical architecture of native cellulose hydrogels Carbohydrate Polymers 147:542-555
696 Martinez-Sanz M, Pettolino F, Flanagan B, Gidley MJ, Gilbert EP (2017) Structure of cellulose
697 microfibrils in mature cotton fibres Carbohydrate polymers 175:450-463
698 Martínez-Sanz M, Vicente AA, Gontard N, Lopez-Rubio A, Lagaron JM (2015b) On the extraction of
699 cellulose nanowhiskers from food by-products and their comparative reinforcing effect on a
700 polyhydroxybutyrate-co-valerate polymer Cellulose 22:535-551
701 Mathew AP, Oksman K, Sain M (2005) Mechanical properties of biodegradable composites from poly
702 lactic acid (PLA) and microcrystalline cellulose (MCC) Journal of applied polymer science
703 97:2014-2025
704 Oehme DP, Downton MT, Doblin MS, Wagner J, Gidley MJ, Bacic A (2015) Unique Aspects of the
705 Structure and Dynamics of Elementary Iβ Cellulose Microfibrils Revealed by Computational
706 Simulations Plant physiology 168:3-17
707 Oh SY, Yoo DI, Shin Y, Seo G (2005) FTIR analysis of cellulose treated with sodium hydroxide and
708 carbon dioxide Carbohydrate Research 340:417-428
709 Park S, Johnson D, Ishizawa C, Parilla P, Davis M (2009) Measuring the crystallinity index of cellulose
710 by solid state 13C nuclear magnetic resonance Cellulose 16:641-647 doi:10.1007/s10570-
711 009-9321-1
712 Pauly M, Albersheim P, Darvill A, York WS (1999) Molecular domains of the cellulose/xyloglucan
713 network in the cell walls of higher plants The Plant Journal 20:629-639
714 Plackett D, Anturi H, Hedenqvist M, Ankerfors M, Gällstedt M, Lindström T, Siró I (2010) Physical
715 properties and morphology of films prepared from microfibrillated cellulose and
716 microfibrillated cellulose in combination with amylopectin Journal of applied polymer
717 science 117:3601-3609
718 Polyakova A, Liu R, Schiraldi D, Hiltner A, Baer E (2001) Oxygen-barrier properties of copolymers
719 based on ethylene terephthalate Journal of Polymer Science Part B: Polymer Physics
720 39:1889-1899
721 Ray B, Lahaye M (1995) Cell-wall polysaccharides from the marine green alga Ulva “rigida”(Ulvales,
722 Chlorophyta). Extraction and chemical composition Carbohydrate Research 274:251-261
723 Reising AB, Moon RJ, Youngblood JP (2012) Effect of particle alignment on mechanical properties of
724 neat cellulose nanocrystal films J Sci Technol For Prod Process 2:32-41

Rodionova G, Lenes M, Eriksen Ø, Gregersen Ø (2011) Surface chemical modification of microfibrillated cellulose: improvement of barrier properties for packaging applications Cellulose 18:127-134
Sánchez-González L, Vargas M, González-Martínez C, Chiralt A, Cháfer M (2009) Characterization of edible films based on hydroxypropylmethylcellulose and tea tree essential oil Food Hydrocolloids 23:2102-2109 doi:https://doi.org/10.1016/j.foodhyd.2009.05.006
Seoane IT, Fortunati E, Puglia D, Cyras VP, Manfredi LB (2016) Development and characterization of bionanocomposites based on poly (3-hydroxybutyrate) and cellulose nanocrystals for packaging applications Polymer International 65:1046-1053
Siddhanta A et al. (2009) Profiling of cellulose content in Indian seaweed species Bioresource technology 100:6669-6673
Singh S, Gaikwad KK, Park S-I, Lee YS (2017) Microwave-assisted step reduced extraction of seaweed (Gelidiella aceroso) cellulose nanocrystals International journal of biological macromolecules 99:506-510
Siqueira G, Abdillahi H, Bras J, Dufresne A (2010) High reinforcing capability cellulose nanocrystals extracted from Syngonanthus nitens (Capim Dourado) Cellulose 17:289-298
Sun X, Xu F, Sun R, Fowler P, Baird M (2005) Characteristics of degraded cellulose obtained from steam-exploded wheat straw Carbohydrate research 340:97-106
Thomas LH et al. (2013) Structure of cellulose microfibrils in primary cell walls from collenchyma Plant physiology 161:465-476
Wada M, Sugiyama J, Okano T (1993) Native celluloses on the basis of two crystalline phase (Iα/Iβ) system Journal of Applied Polymer Science 49:1491-1496
Wang T, Park YB, Cosgrove DJ, Hong M (2015) Cellulose-Pectin Spatial Contacts Are Inherent to Never-Dried Arabidopsis Primary Cell Walls: Evidence from Solid-State Nuclear Magnetic Resonance Plant Physiology 168:871-884 doi:10.1104/pp.15.00665
Whitney SE, Brigham JE, Darke AH, Reid JG, Gidley MJ (1998) Structural aspects of the interaction of mannan-based polysaccharides with bacterial cellulose Carbohydrate Research 307:299-309
Yamazawa A, Iikura T, Shino A, Date Y, Kikuchi J (2013) Solid-, Solution-, and Gas-state NMR Monitoring of 13C-Cellulose Degradation in an Anaerobic Microbial Ecosystem Molecules 18:9021